eng

MDPI

Article

Design and Experimental Validation of Wireless Electric Vehicle Charger Control Using Genetic Algorithms and Feedforward Artificial Neural Network

Marouane El Ancary *, Abdellah Lassioui *, Hassan El Fadil, Yassine El Asri, Anwar Hasni and Soukaina Nady

Ingénierie des Systèmes Avancés (ISA) Laboratory, National School of Applied Sciences (ENSA), Ibn Tofail University, Kenitra 14000, Morocco; elfadilhassan@yahoo.fr (H.E.F.); elasriyassine@yahoo.com (Y.E.A.); hasni.anwar20@gmail.com (A.H.); nady.soukaina@gmail.com (S.N.)

* Correspondence: marouane.elancary@uit.ac.ma (M.E.A.); abdellah.lassioui@uit.ac.ma (A.L.)

Abstract: Integrating electric vehicles (EVs) into the transportation ecosystem is crucial for environmental protection. With the increasing demand for sustainable mobility solutions, wireless power transfer (WPT) systems present a promising method to facilitate the adoption of EVs while reducing carbon footprints. This paper presents a control strategy for the primary side of a WPT charger utilizing a genetic algorithm (GA) combined with a feedforward artificial neural network (ANN). The aim is to optimize charging in constant current (CC) mode and enhance energy transmission efficiency. The proposed approach employs a GA to control the WPT charger, enabling real-time adaptation of charging parameters. The ANN estimates the system's efficiency, ensuring optimal performance during the charging process. The developed control strategy significantly improved energy transfer efficiency and system stability. Simulation results demonstrate the effectiveness of this new approach, achieving an efficiency of 89.32% in challenging situations of loss of communication with the vehicle. To validate the design procedure, an experimental prototype was constructed, operating at an operational frequency of 85 kHz. Experimental results confirm the proposed design methodology.

Keywords: genetic algorithms; feedforward ANN; electric vehicles; battery charging; wireless power transfer

check for updates

Academic Editor: Thaiyal Naayagi Ramasamy

Received: 31 December 2024
Revised: 15 February 2025
Accepted: 19 February 2025
Published: 21 February 2025

Citation: El Ancary, M.; Lassioui, A.; El Fadil, H.; El Asri, Y.; Hasni, A.; Nady, S. Design and Experimental Validation of Wireless Electric Vehicle Charger Control Using Genetic Algorithms and Feedforward Artificial Neural Network. *Eng* **2025**, *6*, 43. https://doi.org/10.3390/eng6030043

Copyright: © 2025 by the authors. Licensee MDPI, Basel, Switzerland. This article is an open access article distributed under the terms and conditions of the Creative Commons Attribution (CC BY) license (https://creativecommons.org/licenses/by/4.0/).

1. Introduction

Climate change is one of the most pressing challenges facing humanity today. Its effects are already being felt on a global scale, altering ecosystems and threatening biodiversity. Rising temperatures, caused mainly by greenhouse gas emissions resulting from human activities, are having a series of environmental consequences. These include the melting of glaciers, rising sea levels, and the intensification of extreme weather events such as hurricanes, droughts, and floods [1,2]. The transport sector and road transport, in particular, plays a major role in accelerating climate change. Accounting for a significant proportion of global greenhouse gas emissions, road transport is mainly dependent on fossil fuels, such as petrol and diesel [3,4]. This dependence contributes to rising concentrations of carbon dioxide (CO_2) in the atmosphere, a key factor in global warming. Motor vehicles, whether used to transport passengers or goods, emit not only CO_2 but also other atmospheric pollutants such as nitrogen oxides (NOx) and fine particles [5,6]. These emissions have harmful effects on air quality, aggravating public health problems

and impacting ecosystems. Urban areas in particular suffer from high levels of pollution, with consequences for both human health and the environment [7,8].

To mitigate these effects, it is essential to promote more sustainable transport solutions, such as electric vehicles (EVs), car sharing, and public transport systems. By reducing our dependence on fossil fuels and improving energy efficiency, it is possible to reduce the carbon footprint of road transport and contribute to the fight against climate change. In this context, the adoption of EVs is a crucial step toward addressing these environmental challenges. By replacing internal combustion vehicles with electric models, it is possible to significantly reduce the greenhouse gas emissions associated with transport [9]. However, to maximize the positive impact of EVs, it is crucial to encourage their uptake in all areas of transport, from private transport to food and goods supply chains. To facilitate this transition, the development of optimal and efficient charging solutions is essential [10]. A well-designed charging infrastructure must be accessible, fast, and reliable, to meet the diverse needs of EV users. This includes the installation of charging stations in strategic locations, such as urban areas, petrol stations, and along major roads. In addition, innovative technologies such as wireless charging and fast-charging systems can help reduce downtime and improve the overall user experience [11].

Wireless chargers represent an innovative and sustainable solution for powering EVs. By enabling charging without a physical connection, these systems improve convenience and accessibility, which can encourage wider adoption of EVs [12]. There are two main types of Wireless Power Transfer (WPT) technology: static WPT, which enables stationary charging, and dynamic WPT, which offers the possibility of charging vehicles in motion, opening up new opportunities for integrating EVs into transport infrastructures [13]. Scientists are also paying particular attention to WPT chargers for intelligent vehicles, which require charging solutions adapted to their advanced technological characteristics. The standardization of wireless charging methods is facilitated by standards such as SAE J2954, which establishes clear guidelines for the interoperability and safety of wireless charging systems. Research is currently focused on exploring renewable energy sources to power WPT chargers [12,14]. Integrating these sources, such as solar or wind power, into wireless charging systems can not only reduce the carbon footprint of EVs but also contribute to a more sustainable and resilient electricity grid. By combining WPT technology with renewable energies, it is possible to create a charging ecosystem that supports the transition to greener modes of transport [15].

Figure 1 shows a simplified WPT system comprising two main parts: the vehicle-side part and the ground-side part. Energy transfer occurs wirelessly through a magnetic field generated by underground transmitting coils and received by coils positioned beneath the vehicle. To ensure efficient energy transfer to the electric vehicle (EV) battery, a control system is necessary to regulate the energy flow [16]. Wireless chargers can be powered flexibly, either via the traditional electricity grid or from renewable energy sources such as photovoltaic or wind power. This versatility means that a variety of energy resources can be used to power charging systems, contributing to a more sustainable energy transition [17]. Integrating these chargers into microgrids or smart grids offers additional opportunities to optimize energy use. These smart grids enable dynamic interaction between vehicles, charging infrastructure, and the electricity grid [18]. For example, G2V (Grid-to-Vehicle) systems allow vehicles to be charged from the grid, while V2G (Vehicle-to-Grid) systems allow vehicles to send the energy stored in their batteries back to the grid during periods of high demand [19]. Similarly, V2H (Vehicle-to-Home) systems enable the energy from an electric vehicle to be used to power domestic appliances, offering a home energy management solution [20]. This integration not only promotes energy efficiency, but also enables better management of renewable resources, by balancing energy supply and

demand. According to the SAE J2954 standard [21], WPT systems are classified into several power levels: low power (up to 1 kW) for small devices, medium power (1 kW to 7.7 kW) for light EVs, high power (7.7 kW to 22 kW) for passenger EVs, and heavy-duty vehicles, and very high power (above 22 kW) for huge vehicles like buses and trucks. This categorization helps standardize WPT systems for various applications, ensuring compatibility and efficiency in EV charging infrastructure.

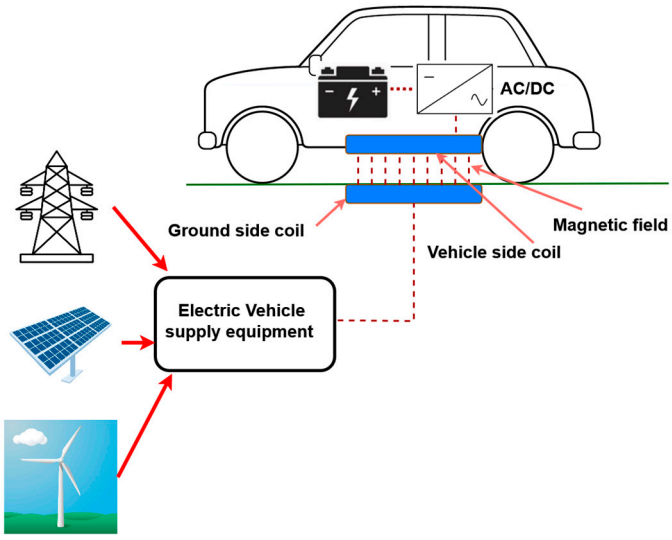


Figure 1. WPT charging system.

To control WPT chargers, several approaches have been proposed in the scientific literature [22]. The first approach, primary-side control, allows the wireless charger to be managed from the ground side. This method offers some flexibility, but requires wireless communication between the vehicle side and the ground side, which can be problematic due to interference or communication breaks, thus limiting the accuracy of the control signals. The second approach, secondary-side control, involves managing the charger from the vehicle side by adding additional DC-DC converters on the secondary side [23]. Although this method can offer better-localized control, it often faces challenges, including the fact that some vehicle manufacturers do not allow access to the vehicle's CAN (Controller Area Network) network, making it difficult to implement this strategy. It is also possible to combine these two approaches to achieve hybrid control, enabling more robust and responsive management of the WPT charger [24]. Each method has specific advantages and limitations, and the choice of approach often depends on the requirements of the system and the technical constraints encountered. This diversity of approaches underlines the importance of continuing to look for innovative solutions to optimize the control of wireless charging systems.

The studies in [25,26] suggest transferring data and power simultaneously. This method uses the phase-shifting key technique to transport power and data through the coils. The proposed approach does not require wireless communication cards; however, additional decoding circuitry is needed to process and decode the data received from the ground side, which will increase the cost and complexity. In addition, since the information is transmitted via the magnetic coupler, the presence of iron and electromagnetic waves may alter the proper operation. The authors in [27] propose a model predictive control (MPC) strategy to control the WPT systems to improve the stability and efficiency of power transfer, especially under varying load conditions and coupling coefficients, the implementation of the proposed MPC algorithm may require significant computational resources, which could affect real-time performance. The emphasis in [28] is on managing

variations in output voltage and coupling coefficient, using a simple design and control by integrating a battery management converter on the secondary side, and incorporating a phase shift control on the primary side. The authors propose a double-regulation loop on the primary side and the secondary side. Indeed, the proposed method allows optimal charging, but the addition of DC-DC converters on the secondary side poses a problem both in terms of car manufacturers not providing access to the CAN network as already mentioned, but also the degradation of performance due to the addition of complementary systems as well as the synchronization between the two controls in real time. Also, in the paper [29], the authors propose a control strategy for WPT systems that moves traditional vehicle-side control DC-DC to the transmitter side. This approach allows the determination of mutual inductances independent of misalignment, enabling robust operation, it also allows the elimination of DC-DC converters on the receiver side, simplifying the receiver circuit and reducing size and cost and, finally, it allows the implementation of constant frequency operation to improve efficiency. But for this additional calibration circuits are required on the load ends. The authors in [30,31] propose a method for controlling the WPT charged from the primary side while identifying the load from the measurement of the voltage and current between the primary coil.

Regarding the integration of artificial intelligence (AI) and machine learning (ML) into WPT systems, recently, there has been an increased focus on this area to dig deeper to assess the performance of AI in this field. In this context, the authors in [32] propose a method for optimizing WPT design parameters such as coils and compensation capacitors. A genetic algorithm (GA) is used for this purpose and the results show an efficiency of 82% with a transmitter power of 173.89 mW. This solution is for low-power applications with a reduced air gap between the primary and secondary sides of 10 mm. Also, the study in [33] used a GA to optimize circular spiral coils for WPT. The aim is to find the optimum values for the mutual inductance between the transmitting and receiving coils. When optimizing circular coils, the most important parameters are the number of coil turns and the pitch between the turns. In the paper [34], the authors propose a method for optimizing the linear quadratic regulator (LQR) controller by updating offline the parameters using GA. The approach is tested under normal conditions via simulation without any practical validation of the method to prove its applicability in real scenarios. In [35], the authors used an artificial neural network (ANN) to estimate the mutual inductance and the load resistance—the method proposed for low power and low air gap. In this paper, the resonant frequency is 100 kHz, and the input voltage is of the order of 10 V which is far from being applicable in automotive applications; additionally, the authors used a resistor as a load. Also, in this study [36], the authors used a convolutional neural network (CNN) to predict the performance of a pair of coupled coils. The optimized parameters are the spatial distribution of the magnetic field, the quality factor, the value of the inductance, the value of the mutual inductance, as well as the number of turns, and the wire diameter of the coils. Also, in this paper [37], the authors used a CNN to estimate mutual inductance. To train the CNN, the method consists of applying to the input of the CNN an image depicting the geometry of two coils that are partially misaligned. The CNN then processes and gives the estimated value of the inductance. This study was conducted in the context of dynamic WPT, where at any given moment the two coils are in motion to each other.

We can see from the literature review provided that the control of the primary side of the WPT charger is extensively studied and employed due to its advantages of simplicity and cost-effectiveness, which are significant strengths for the deployment of this charging method. However, these techniques either rely on load identification or, in addition to primary control, incorporate DC-DC converters on the secondary side to ensure the proper functioning of the EV's battery charging process. Furthermore, there is a gap in

the integration of AI and ML in the control of this type of WPT charger especially for automotive applications.

The new contribution of this paper lies in the integration of AI into the control of the WPT charger from the primary side, leveraging the advantages of ML in control systems. The proposed approach involves combining a GA controller with a feedforward ANN to estimate efficiency, as this efficiency varies with the state-of-charge (SOC) of the battery. Furthermore, it is essential to maintain minimal communication between the primary and secondary sides to protect the battery from overcharging and temperature increases. This is the first time that a GA and an ANN have been combined for the control of WPT from the ground side in challenging loss-of-communication situations, representing a significant advancement in the development of this charging method, ultimately facilitating the increased adoption of EVs to protect the environment.

The remaining sections of this paper are organized as follows: Section 2 introduces the WPT charger, its modeling, and the equivalent circuit representation. Section 3 illustrates the proposed control strategy. Section 4 presents the results and discussion of the control technique and its performance based on simulation results, while Section 5 covers the experimental validation of the control technique and the corresponding experimental results. A discussion is presented in Section 6. Finally, Section 7 presents conclusions and future research directions.

2. System Structure and Circuit Model

This section is dedicated to the description of the WPT for EVs charger. The wireless charging process is summarized schematically in SAE J2954 standard [21] and can be divided into two subsystems, as shown in Figure 2: the primary side, also known as the ground-side-assembly (GSA), and the secondary side, also known as the vehicle-side-assembly (VSA) [38]. A high-frequency DC-AC converter, operating at 85 kHz as recommended by SAE J2954, generates a time-varying voltage [39]. The transmitter coil, powered by the converter, generates a time-varying magnetic flux (MF) at the same resonance frequency, hence the name "magnetic resonance charger". This magnetic flux is transmitted wirelessly and transported to the receiver coil. The standard voltages and currents required by the battery are obtained by rectifying and filtering the secondary coil voltage.

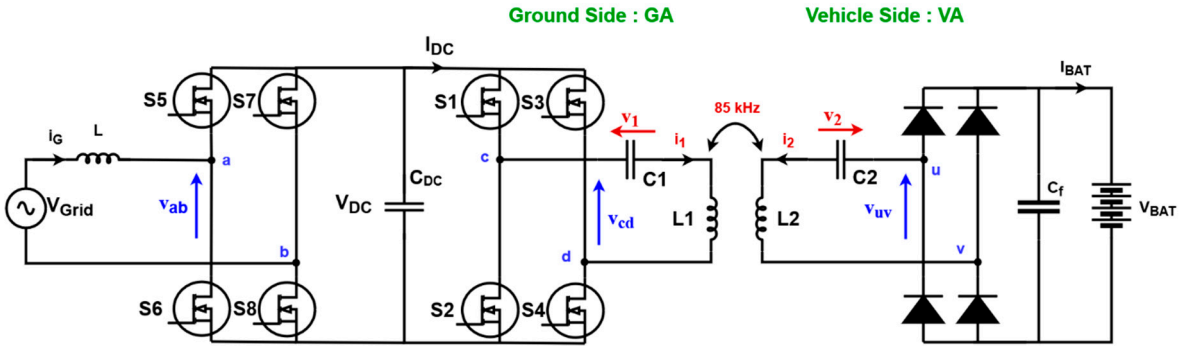


Figure 2. WPT charger circuit.

The development of an accurate analytical model for the wireless charger is very important in the analysis and understanding of the phenomena that occur in the WPT charger, the Power Factor Correction (PFC) stage is not included in this paper, and the analysis is limited to the system components between the DC bus and the vehicle battery. In addition, the battery is modeled by a resistor r_b in series with an open circuit voltage v_{OC}; this model, equivalent to the battery, is accurate and can be it in real situations where

the resistor r_b is not constant all over the charging process. Once the Kirchhoff rules have been applied to the circuit in Figure 2, the results are presented in Equations (1)–(5):

$$v_{CD} = v_1 + L_1\frac{di_1}{dt} - M\frac{di_2}{dt} \tag{1}$$

$$M\frac{di_1}{dt} = v_{uv} + v_2 + L_2\frac{di_2}{dt} \tag{2}$$

$$i_1 = C_1\frac{dv_1}{dt} \tag{3}$$

$$i_2 = C_2\frac{dv_2}{dt} \tag{4}$$

$$i_{BAT} = |i_2| = \frac{v_0 - v_{OC}}{r_b} + C_f\frac{dv_0}{dt} \tag{5}$$

where i_1 and i_2 are the currents in the primary-side and secondary-side coils; L_2 and L_2 are the inductances of the primary and secondary side coils; M is the mutual inductance between the coils; v_{cd} is the inverter output voltage; v_1 and v_2 are, respectively, the voltage across the primary and secondary side compensation capacitors; v_{uv} and v_0 are, respectively, the voltage at the input and output of the secondary-side rectifier; and C_f is the filtering capacitor of the secondary side.

From (1) to (5), the following state space model is obtained:

$$x = [v_1, v_2, i_1, i_2, v_0]^T = [x_1, x_2, x_3, x_4, x_5]^T \tag{6}$$

$$\dot{x}_1 = \frac{1}{C_1}x_3 \tag{7}$$

$$\dot{x}_2 = \frac{1}{C_2}x_4 \tag{8}$$

$$\dot{x}_3 = \frac{1}{K_1}(v_{cd} - x_1) - \frac{1}{K_2}(x_2 - \mathrm{sgn}(x_4)x_5) \tag{9}$$

$$\dot{x}_4 = \frac{1}{K_2}(v_{cd} - x_1) - \frac{1}{K_3}(x_2 - \mathrm{sgn}(x_4)x_5) \tag{10}$$

$$\dot{x}_5 = \frac{1}{C_f}\mathrm{sgn}(x_4)x_4 - \frac{x_5 - v_{OC}}{C_f r_b} \tag{11}$$

where $K_1 = \frac{L_1L_2 - M^2}{L_2}$, $K_2 = \frac{L_1L_2 - M^2}{M^2}$, $K_3 = \frac{L_1L_2 - M^2}{L_1}$ and $\mathrm{sgn}(x) = 1$ when $x > 0$, $\mathrm{sgn}(x) = -1$ when $x < 0$ and $\mathrm{sgn}(x) = 0$ when $x = 0$.

The RMS value of the inverter output voltage can be expressed using the Fourier series as [40]:

$$V_{RMS} = \frac{2\sqrt{2}}{\pi}V_{DC}\cos(\frac{\alpha}{2}) \tag{12}$$

where α represents the phase shift angle or delay between the arms of the inverter on the primary side. Figure 3 clearly shows the control signals and the output waveforms of the phase-shifted bridge inverter. As can be seen, the switches, S1 (S3) and S2 (S4), complement each other, and the duty cycle of the control signals varies the signals. Depending on the conduction of the switches, v_{cd} can be zero, $+V_{DC}$, or $-V_{DC}$. By adjusting the width of v_{cd} with the angle α, which varies from 0 to 180°, the amplitude of its fundamental is entirely related to the angle α and can be described as follow [40]:

$$v_{cd_f} = \frac{4}{\pi}V_{DC}\cos(\frac{\alpha}{2})\sin(\omega t) \tag{13}$$

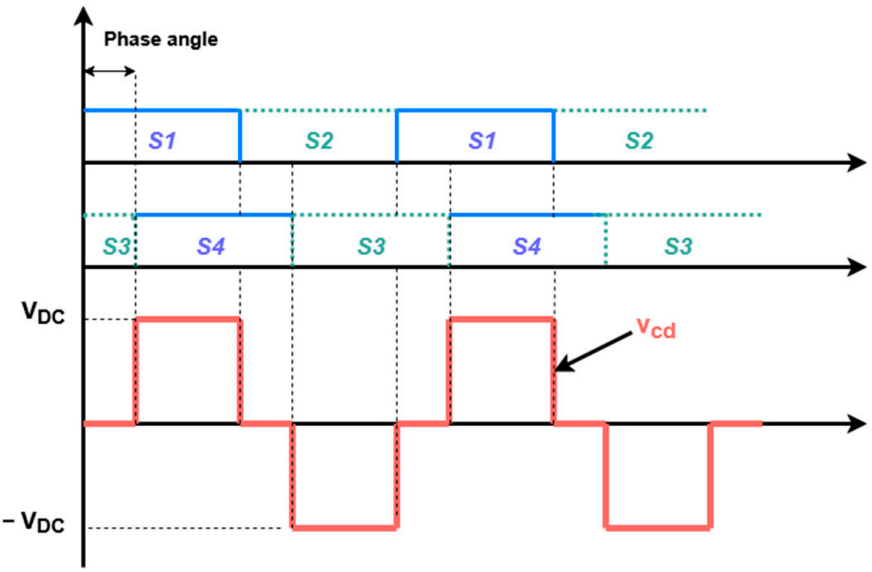


Figure 3. Waveforms of phase shift control method.

Phase shift control is often preferred by WPT systems over pulse width modulation (PWM) due to its superior efficiency and simplicity of control. It optimizes power transfer by adjusting the phase difference between the control signals of the primary and secondary coils, thereby reducing reactive power losses. Moreover, phase shift control minimizes electromagnetic interference by operating at resonant frequencies and improves thermal performance, thereby increasing system reliability.

3. The Proposed Control Approach

This section is devoted to the design of a novel control strategy for a WPT charger. The proposed hybrid control approach, which integrates a feedforward ANN and GA controller, is specifically designed to regulate battery current during constant current (CC) charging mode. This focus on CC mode aligns with the practical charging requirements of EVs, where batteries are typically charged at a constant current until reaching approximately 80% of their SOC, after that, we transitioned into constant voltage (CV) mode.

Notably, the control system is entirely located on the primary side of the WPT system, minimizing complexity on the vehicle side and reducing the weight of the EV; also, the minimization of the control circuits on board reduces the power consumption for such systems which greatly improves the autonomy of the batteries. To ensure safety and accommodate variations in system parameters caused by grid instability or misalignment between the vehicle and charging station, a minimal communication link is established.

This control approach of the WPT charger is based on the estimated power transfer efficiency η. In this case, the WPT system is firstly operated in an open-loop mode in which the efficiency is calculated based on the measured powers in the ground side and vehicle side. Then, based on the estimated efficiency, the WPT system will be operated in a closed-loop mode where the battery charging current is controlled indirectly through the control of the average DC current on the ground side $I_{DC,avg}$. The main advantage of this control approach is that wireless data communication is solely needed during the identification phase of the efficiency.

The efficiency is calculated as follows:

$$\eta = \frac{P_{out}}{P_{in}} = \frac{I_{Bat} * V_{Bat}}{I_{DC,avg} * V_{DC}} \tag{14}$$

The reference of the average DC current on the ground side is calculated based on the desired battery charging current and the estimated efficiency as follows:

$$I_{DC,avg,reference} = \frac{I_{Bat,reference} * V_{Bat}}{\eta * V_{DC}} \quad (15)$$

Figure 4 shows this control approach of the WPT charger which is based on the estimated power transfer efficiency η. To accurately estimate the average DC current, we trained a feedforward ANN estimator using simulated data. The ANN was designed to predict the system efficiency based on calculated DC current I_{DC} and voltage V_{DC} values, in addition to battery current I_{BAT} and voltage V_{BAT}, which vary with the battery's internal resistance as the charging process progresses.

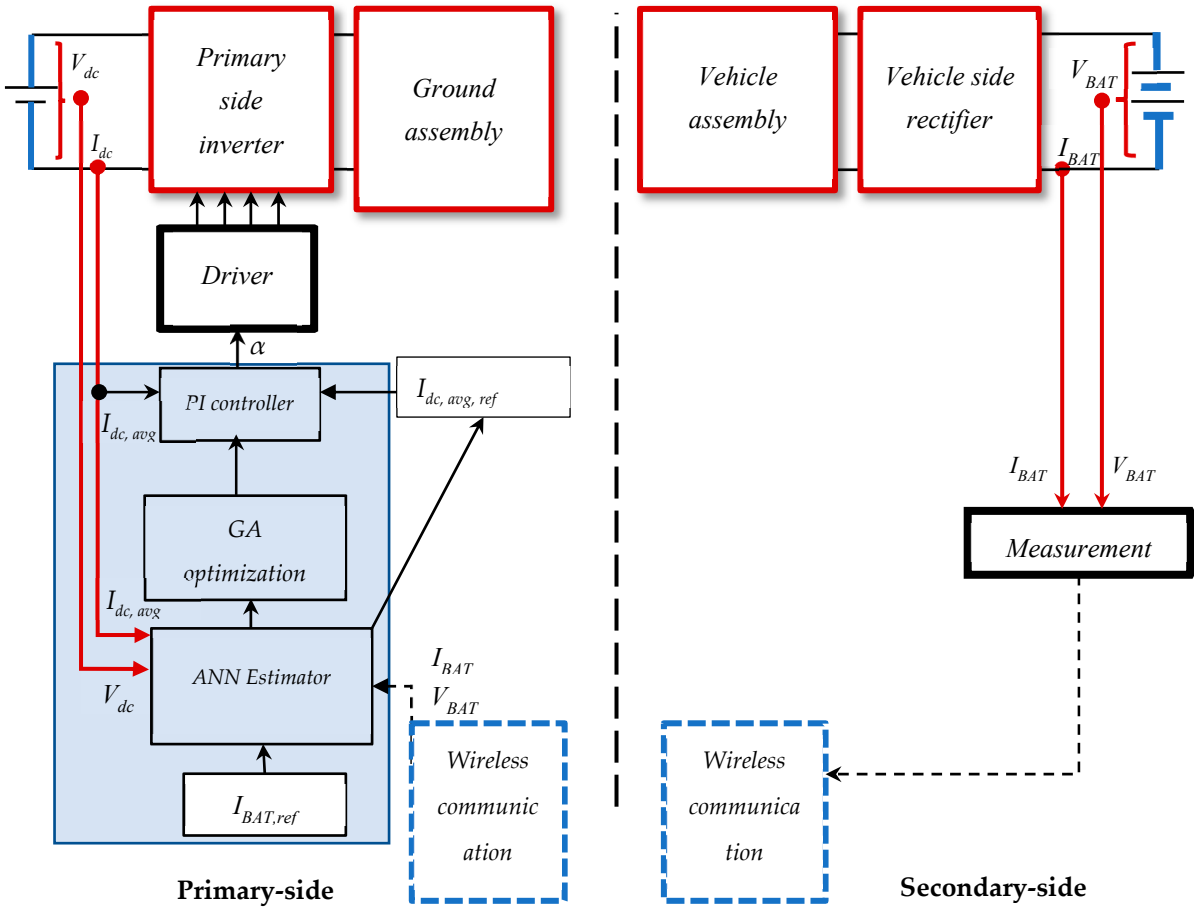


Figure 4. The general concept of the ground-side control approach of the WPT charger based on efficiency estimation using ANN and GA-based control.

3.1. GA Optimization

GA optimization has become an effective approach for tuning proportional–integral-derivative (PID) controllers due to its ability to efficiently explore large and complex search spaces. Traditional PID tuning methods, such as Ziegler–Nichols, often struggle to achieve optimal performance for non-linear or time-varying systems, as they rely on approximations and fixed rules [41]. GA, as an evolutionary optimization technique, mimics the process of natural selection and adapts over generations to identify optimal solutions. By applying GA to PI tuning, the proportional, integral, and derivative gains can be automatically optimized based on a defined fitness function, which could be related to performance criteria such as overshoot, settling time, or steady-state error. This method ensures a more

adaptive and accurate tuning process that adjusts to the system's specific dynamics. In GA optimization, the fitness function plays a critical role in evaluating the performance of potential solutions. Various types of fitness functions can be employed, including the Mean Squared Error (MSE), Integral of Time multiplied by Absolute Error (ITAE), Integral of Absolute Magnitude of the Error (IAE), Integral of the Squared Error (ISE), and Integral of Time multiplied by the Squared Error (ITSE). Each of these functions provides a different perspective on error minimization and system performance. The fitness of the chromosome is decided by the value of the fitness function. The main objective of the fitness function is to minimize the error [42].

MATLAB R2024a's optimization tool is used to simulate GA optimization. Before being entered into the optimization tool, the code that defines the fitness function is written. The fitness function is the ITAE function. *Kp* and *Kd* are the fitness function's unknown output parameters. Table 1 displays the other input parameters.

Table 1. Parameters of GA.

GA Parameters	Description	Value/Method
Population Size	Number of individuals in the population.	30
Max Generations	Maximum number of generations to evolve.	60
Selection Function	Method to select parents for reproduction.	Tournament
Crossover	Method to combine two parents to create offspring.	Arithmetic
Fraction Function	Fraction of the population for crossover.	0.8
Mutation Function	Method to introduce diversity in offspring.	Uniform
Mutation Rate	Probability of mutation per gene.	0.15
Performance Index	Fitness function.	ITAE
Variable Bounds [*Kp*, *Ki*]	The range within which the GA searches for optimal values.	[0, 5; 10, 10000]

The flowchart of the GA process is outlined in Figure 5. The general execution procedure for GA is as follows: Initialization involves creating a starting pool of potential solutions (*Kp* and *Ki* pairs) within specified limits. Each candidate is assessed using an objective function. The top performing candidates are chosen as parents for the next generation. These parents combine their characteristics to produce offspring through crossover. Random modifications are applied to these offspring during mutation to encourage exploration. This iterative process continues until the algorithm converges on the best *Kp* and *Ki* values, optimizing the system's performance.

The GA fitness function is tailored to assess the performance of the PI controller in the WPT system, in particular, to ensure a CC mode with minimum response time. The suitability function incorporates the following key performance measures:

- e_I: The difference between the desired current $I_{BAT,ref}$ and the battery charging current I_{BAT};
- $t_{r,5\%}$: The time taken for the WPT charger to reach and stabilize within ±5% of the desired charging current.

The fitness function F is formulated as follows:

$$F = \omega_1 \,.\, ITAE(e_I) \;+\; \omega_2 \,.\, t_{r,5\%} \tag{16}$$

where

$ITAE(e_I)$ is the Integral of Time multiplied by the Absolute Error of the battery current error;

$t_{r,5\%}$ is the response time <0.01 s;
ω_1, ω_2 are weighting factors.

The objective of the optimization problem is to minimize the fitness function F to achieve optimal PI controller gains (*Kp* and *Ki*) for the WPT system, ensuring CC charging mode with minimal response time and zero error. The constraints include maintaining the batter charging current I_{BAT} close to the reference current $I_{BAT,ref}$ for CC mode, minimizing the response time $t_{r,5\%}$ to ensure fast convergence, and cancelling the static error in a permanent regime. The decision variables are the proportional gain *Kp* and integral gain *Ki* of the PI controller. Mathematically, the problem is formulated as follows:

$$\min_{K_P,K_i} F(K_P, K_I) \tag{17}$$

which is subject to

$$I_{BAT,ref} \approx I_{BAT} \tag{18}$$

$$t_{r,5\%} \leq t_{\max} = 0.01 \text{ s} \tag{19}$$

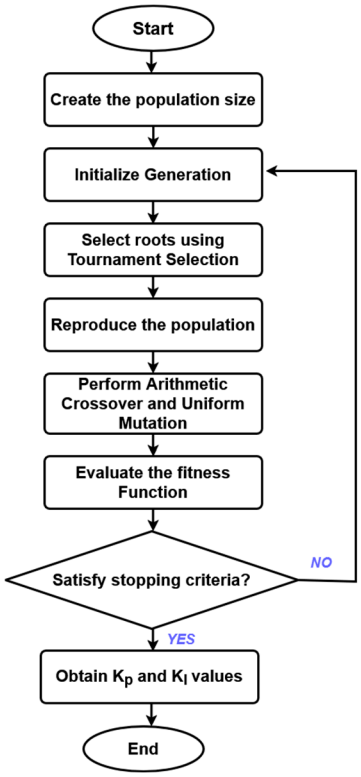


Figure 5. Flowchart of GA process.

We conducted numerous tests and simulations to determine the optimal parameters for the GA, including the boundary limits. We observed that when these limits are narrower, the GA converges on solutions more quickly. However, the process is stopped after a certain number of cycles or generations to balance computation time and solution quality. The GA is activated only at the end of a vehicle's charge after a prolonged break in communication with the vehicle side. To speed up the execution of the algorithm, we used an approach based on parallelized fitness evaluations by using all 16 CPU cores and 32 threads to evaluate multiple individuals simultaneously. We also have implemented early stopping to accelerate the process by terminating the GA if any individual in the population meets the threshold criteria of the fitness value. The optimal running time

obtained was approximately 6 min, using 16 CPU cores (Intel Core i9-12900K, Santa Clara, CA, USA), 64 GB RAM (Corsair Vengeance, Fremont, CA, USA), and a GPU with 24 GB VRAM (NVIDIA GeForce RTX 3090, Santa Clara, CA, USA).

3.2. ANN Efficiency Estimation

The ANN model is inspired by the functioning of biological neurons. In contrast to traditional algorithms, ANNs learn from input data and transform it into knowledge in a manner similar to that of the human brain. ANNs are architecturally formed by interconnected elementary units named neurons. The structure of neural networks commonly follows a layered structure. The network architecture is defined by the number of layers and the number of neurons within each layer [43]. The ANN estimator employs a three-layer structure, as illustrated in Figure 6.

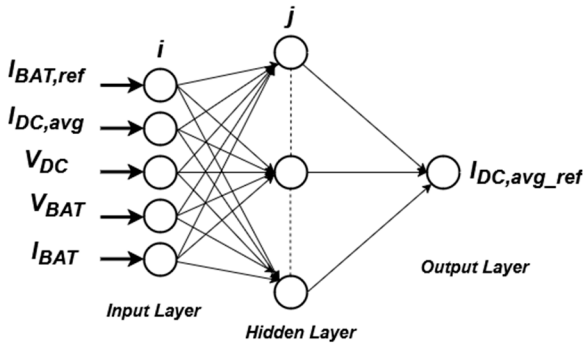


Figure 6. Structure of the feedforward ANN estimator.

To predict the $I_{DC,avg,ref}$ value to be applied at the controller input as a new reference in the event of no communication with the vehicle, we use a multi-layer perceptron (MLP), as shown in Figure 6. We can clearly see that the ANN is able to estimate $I_{DC,avg,ref}$ by indirectly estimating efficiency from the inputs applied to the MLP estimator ($I_{BAT,ref}$, $I_{DC,avg}$, V_{DC}, V_{BAT} and I_{BAT}). The cost function for our optimal prediction parameter is the Mean Squared Error (MSE):

$$J(\theta) = \frac{1}{N} \sum_{i=1}^{N} \left(I^{(i)}_{DC,avg,ref_{(predicted)}} - I^{(i)}_{DC,avg,ref_{(actual)}} \right)^2 \quad (20)$$

where

$J(\theta)$ is the cost function to be minimized;
N is the number of training samples;
$I^{(i)}_{DC,avg,ref_{(predicted)}}$ is the reference DC current predicted by the MLP for the i-th input sample;
$I^{(i)}_{DC,avg,ref_{(actual)}}$ is the actual or measured reference DC current for the i-th input sample.
θ represents the parameters (weights and biases) of the MLP.

The L2 regularization is added to the cost function to avoid over-fitting:

$$J(\theta) = \frac{1}{N} \sum_{i=1}^{N} \left(I^{(i)}_{DC,avg,ref_{(predicted)}} - I^{(i)}_{DC,avg,ref_{(actual)}} \right)^2 + \lambda \sum_{j=1}^{K} \theta_j^2 \quad (21)$$

where λ is the regularization parameter and K is the number of parameters in the MLP. The ANN used has (5 neurons in the Input layer, 25 neurons in the hidden layer, and 1 neuron in the output layer), which means that we have $K = 176$ trainable parameters.

For learning, we use stochastic gradient descent to keep the cost function to a minimum. The Adaptive Moment Estimation (ADAM) optimizer is used in our WPT system, with a

learning rate of 0.0001. Using MATLAB, we generated 700,000 samples. With this dataset, we chose 75% randomly for training and the remaining 25% for testing and validation. The ANN model is trained for 500 epochs in total.

4. Simulation Results

To evaluate the performance of our new WPT charger control method, we first carried out simulations using a specialized simulation tool. The simulation parameters are detailed in Table 2. It is important to note that these values are close to those measured during the practical validation phase. This approach ensures that the simulation results closely resemble real-life conditions, which reinforces the reliability and applicability of our conclusions.

Table 2. Parameters used during simulations.

Parameter	Value
DC bus voltage for the primary side V_{DC}	100 V
Self-inductance of the ground side coil L1	416 µH
Self-inductance of the vehicle side coil L2	116 µH
Mutual inductance M	20 µH
Primary side compensation capacitor C1	8.5 nF
Secondary side compensation capacitor C2	30 nF
Resonance frequency f	85 kHz
Battery voltage V_{BAT}	48 V
Battery capacity	100 Ah

In order to check the feasibility of the control approach, a simulation setup has been built in the MATLAB R2024a environment. In this test, the DC side voltage was set to 100 V which is the DC power supply in the laboratory. The obtained simulation results are presented and discussed in the sequel.

The open-loop test gives rise to an efficiency of approximately 89.32%. Based on the latter, the average DC reference currents corresponding to the desired battery charging reference currents of 1 A and 2 A are calculated using (15). The following values are obtained:

$$I_{DC,avg,reference,1} = \frac{I_{Bat,reference,1} * V_{Bat}}{\eta * V_{DC}} = \frac{1 * 52.3}{0.89 * 100} = 0.587 \text{ A} \quad (22)$$

$$I_{DC,avg,reference,2} = \frac{I_{Bat,reference,2} * V_{Bat}}{\eta * V_{DC}} = \frac{2 * 52.3}{0.89 * 100} = 1.175 \text{ A} \quad (23)$$

It can be seen in Figure 7 that the average DC current tracks perfectly its reference. This means, according to the indirect control technique and as shown in Figure 8, that the battery charging current is well regulated to the desired reference. The control signal is plotted in Figure 9 where it can be seen that the latter is stable without any saturation or overshoot at the time the battery reference current was changed. These results show that the control approach provides good performance.

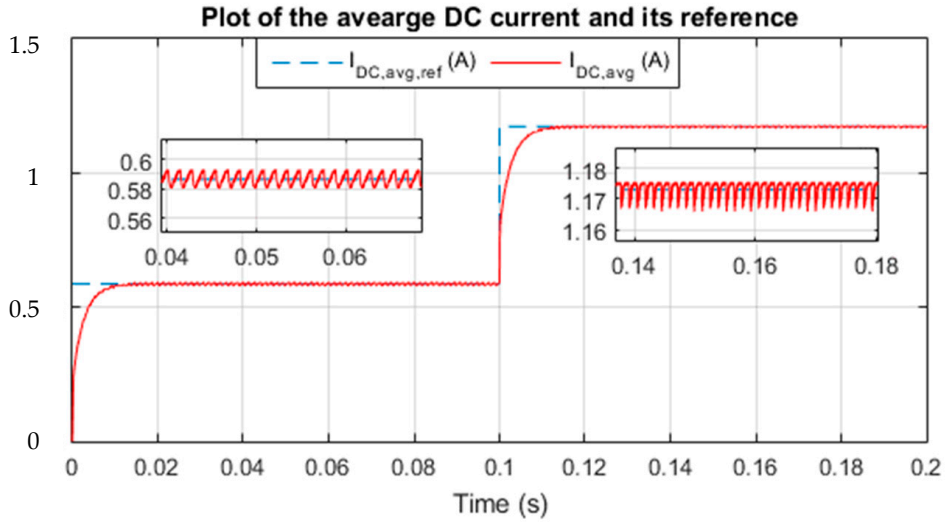


Figure 7. Average DC current and its reference.

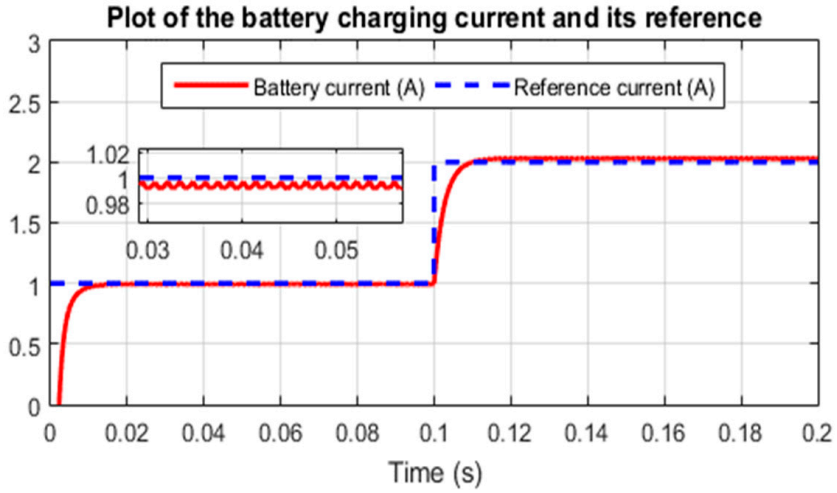


Figure 8. Battery current and its reference.

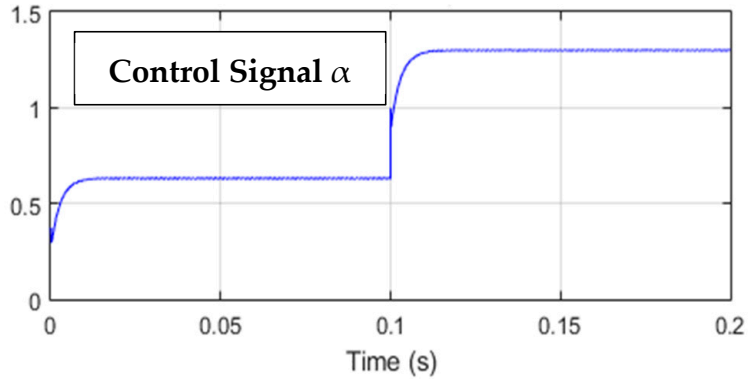


Figure 9. Control signal α(rad).

The evolution of the battery voltage is plotted in Figure 10. Despite the short simulation time, we can notice that this voltage increases during charging operation with a slight step at the time the current was increased from 1 A to 2 A.

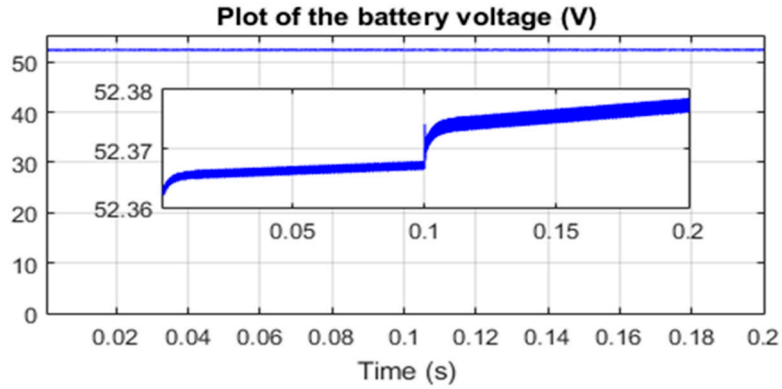


Figure 10. Battery voltage evolution.

Figure 11 shows the input and output power which vary according to the reference current of the WPT charger in the case of a large air gap of 250 mm in the challenging situation of loss of communication with the vehicle. We remark that the efficiency remains constant around a value of approximately 89%. It should be noted that this value will be maintained constant as long as the mutual coupling is not modified.

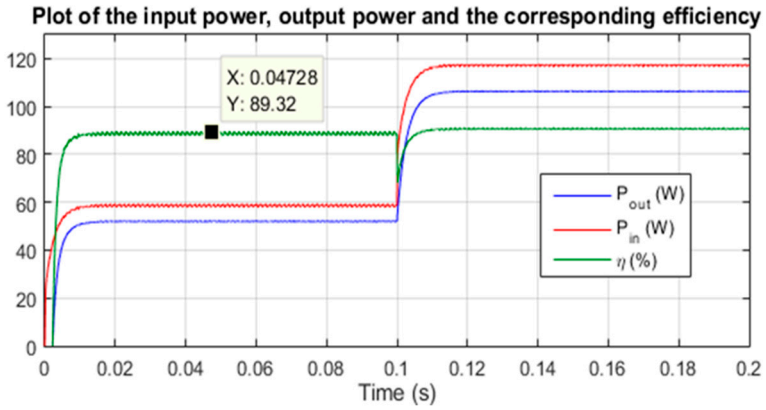


Figure 11. Input power, output power, and the efficiency.

From the simulation results, we can clearly see the effectiveness of the proposed control method. Based on the estimated efficiency from the feedforward ANN, a new $I_{DC,avg,ref}$ is calculated to control the inverter on the primary side. With this approach, the battery charging is ensured in CC mode with free consistent communication from the vehicle side, which makes it possible to manage system operation in the event of communication disruption or communication loss. In addition to all these, the GA controller makes it possible to adapt the gain of the PI controller online whenever parameter updating is required.

To test the effectiveness of our approach, we carried out a comparison test as shown in Figure 12. We applied a reference current of 5 A between 0 s and 0.04 s. Between 0 s and 0.02 s, the communication between the ground side and the vehicle side is assured and we can see that the current in the battery correctly follows the reference current. In the following, between 0.02 s and 0.04 s, a loss of communication occurs, and our approach enables rapid adaptation so that the ANN estimates and gives the new setpoints to the controller, whereas without the ANN, the WPT delivers a maximum current due to saturation of the control signal, which is equal to 1, because the controller no longer receives feedback and therefore the error is maximum, and this is why the controller delivers a

maximum current. The control signal of both methods is illustrated in Figure 13, where we see the saturation of the controller in the absence of the ANN.

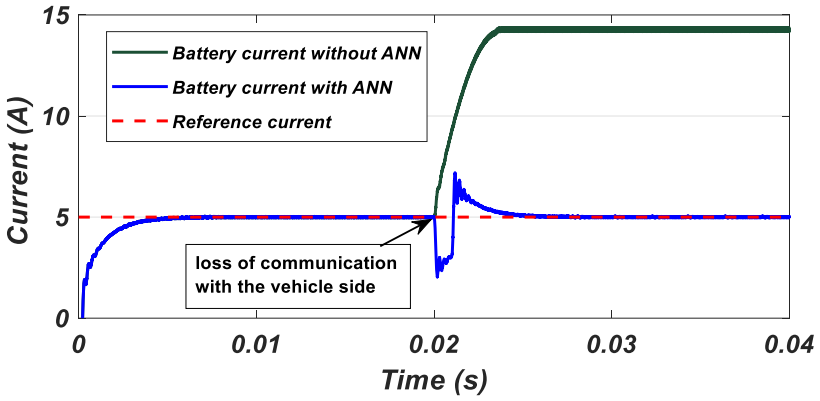


Figure 12. Comparison test in the event of loss of communication with the vehicle side.

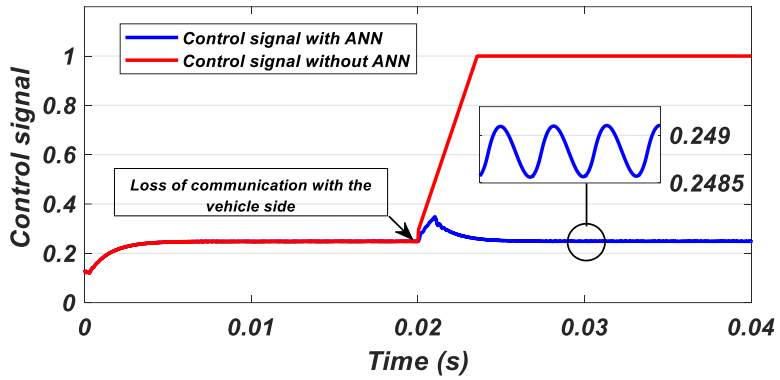


Figure 13. Corresponding control signal in the case of the loss of communication with the vehicle side.

To test the robustness of the proposed method, a test is carried out to evaluate its performance by changing the alignment between the two sides. Figure 14 clearly shows that the system maintains stable operation and continues to track the reference current efficiently, even when the coils are misaligned, and that induces variation in the mutual inductance.

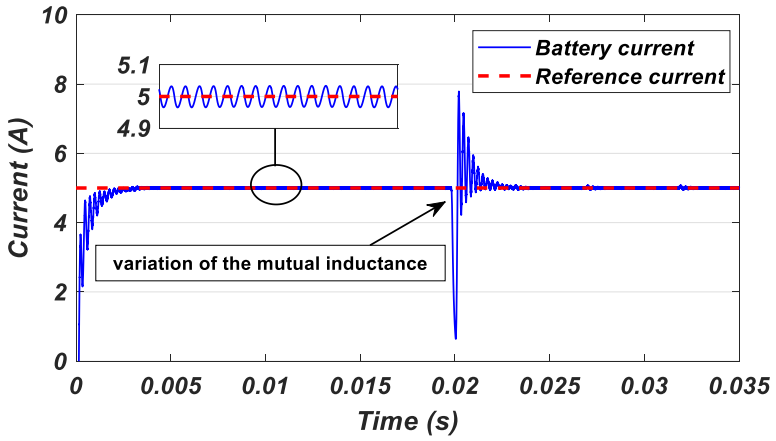


Figure 14. Robustness of the control method under misalignment between coils.

In series compensation, a capacitor is connected in series with the coil, with the same current flowing through both. This capacitor is chosen so that its capacitive reactance

cancels the inductive reactance of the coil at the desired operating frequency. The voltage across the capacitor V_C is given by the formula:

$$V_C = I \cdot X_C \tag{24}$$

where I is the current and X_C is the capacitive reactance. At resonance, X_C is high because the capacitor is chosen to cancel the inductive reactance, and current I is also high due to the low impedance. The combination of high current and high capacitive reactance results in a very high voltage across the capacitor. Figures 15 and 16 show the primary and secondary capacitor voltages and currents in the primary and secondary coils at resonance frequency.

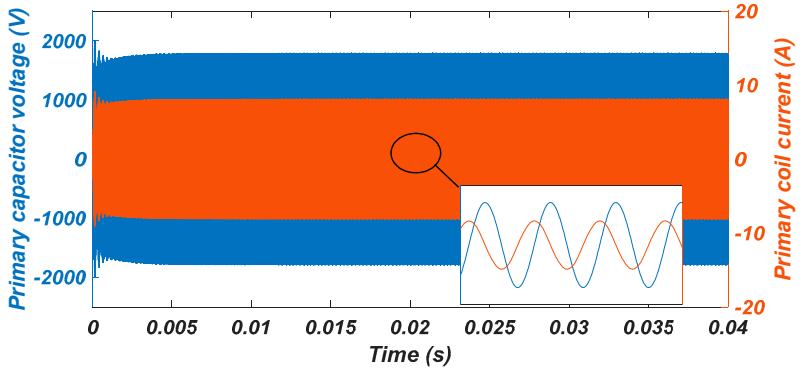


Figure 15. Primary-side capacitor voltage and coil current.

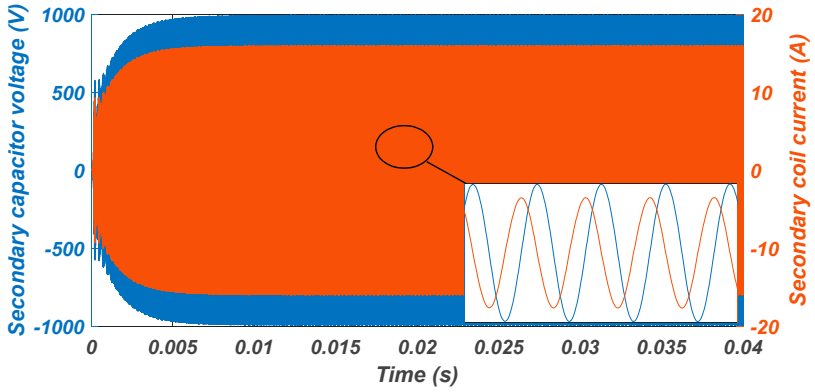


Figure 16. Secondary-side capacitor voltage and coil current.

5. Experimental Validation

The aim of this section is to present the practical validation of the proposed method for controlling the WPT charger, the overall experimental setup is shown in Figure 17. The DC power supply delivers the DC voltage V_{DC} for the HF inverter. This voltage in reality is delivered either by the traditional grid after rectification with a PFC as already shown in Figure 2 or by renewable energies. PFC is essential for improving the efficiency and stability of electricity networks by minimizing reactive power and maximizing the use of active power. It reduces energy losses, lowers the load on transmission and distribution infrastructures, and maintains stable voltage levels, thus guaranteeing a reliable energy supply. In addition, PFC helps utilities comply with regulatory standards, reduces operating costs, and promotes the integration of renewable energy sources by mitigating power-quality issues.

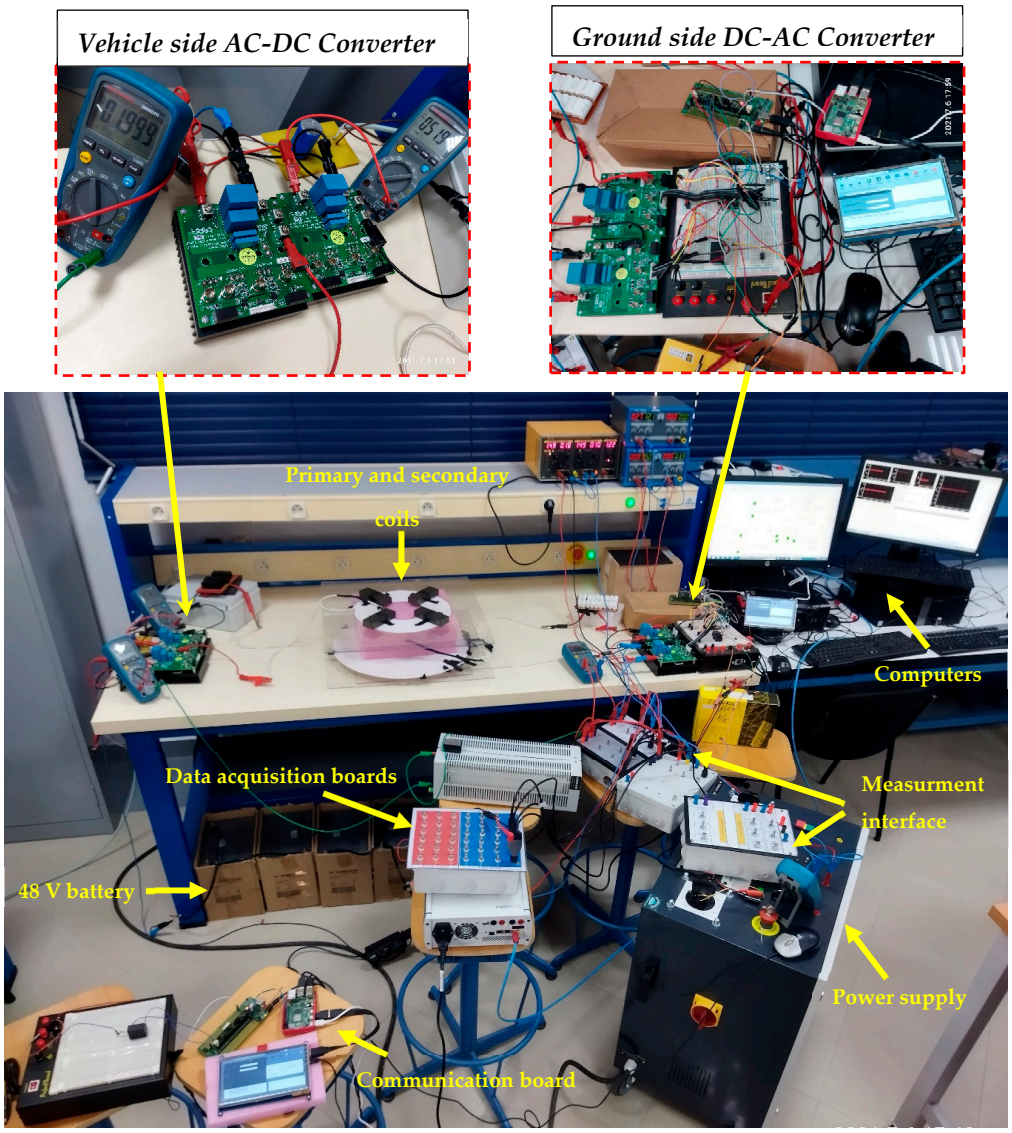


Figure 17. Overall experimental validation setup.

The power converters used in this practical phase are based on silicon carbide (SiC) and galium nitride (GaN) MOSFETs, which are emerging technologies that are best suited to WPT chargers because their performance remains higher even when operating at high frequency and high power. For this purpose, and in view of the 85 kHz resonance frequency of SiC MOSFETs, the use of GaN MOSFETs is recommended by Wolfspeed, Inc., Durham, NC, USA.

The WPT charger works in magnetic resonance mode. This is why we need to add capacitors in series with the primary and secondary coils, knowing that there are different compensation topologies apart from series–series (S-S), but this choice is justified by the fact that the S-S compensation topology allows the compensation capacitors to be sized without influencing the load, This is an important factor, especially in the case of the WPT charger, where the load variation and misalignment between primary and secondary coils are important and, above all, frequent. This is even the main reason for having regulation loops, which must be efficient and robust. Another very important property of S-S topology capacitors is that they can withstand significant voltage peaks due to the resonance and it is therefore preferable to use several capacitors in series and in parallel to form the desired

compensation capacitance calculated, according to the value of the corresponding coil and the working frequency [44,45], hence the choice of capacitors as shown in Figure 18.



Figure 18. Vehicle-side compensation (**Left**) and ground-side compensation (**Right**).

The choice of coil geometries is a very important task as they form the heart of the WPT charger, and for this system, we have chosen the circular geometry due to the uniformity of the magnetic field produced by the primary coil and picked up by the secondary coil; to reduce the proximity and skin effect, the primary and the secondary coils are made of 1050 strand twisted Litz wire. In addition, Mn-Zn ferrite cores from TDK Corporation are also added to guide the flux between the coils as depicted in Figure 19. Detailed design of GSA and VSA coils can be found in [46].

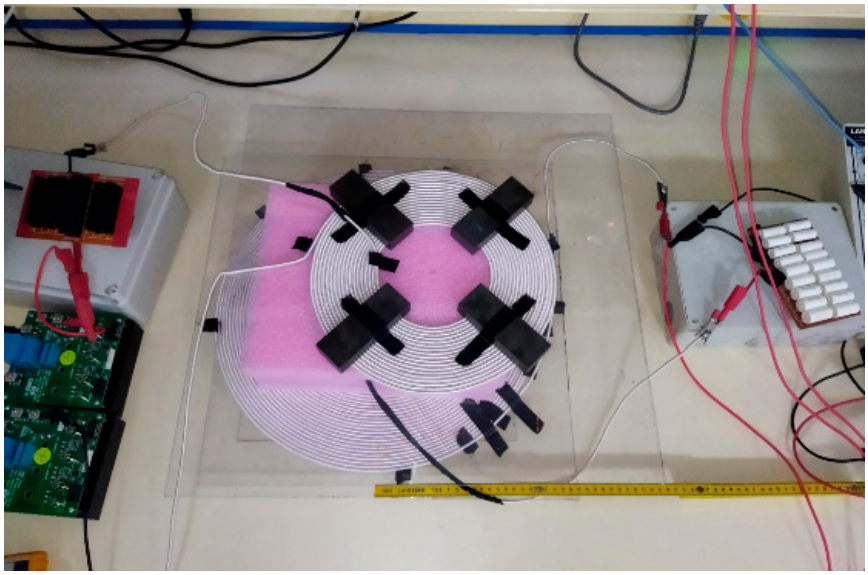


Figure 19. Arbitrary positioning of the coils during the test of the control approach.

Following the SAEJ2954 standard, which imposes a nominal distance between the two coils of 125 mm, and for extreme conditions, we can increase this air gap to 250 mm, because of this distance the system will present a low coupling coefficient and a mutual inductance of about 20 µH. In addition to controlling the system, a TI C2000 f28335 (Texas Instruments, Dallas, TX, USA) control board is used with a Raspberry Pi4-type communication interface (Sony UK Technology Centre, Pencoed, UK) to ensure communication between VSA and GSA for the test. A 48 V battery is employed as the load, in addition to the data acquisition and measurement cards, as illustrated in Figures 17 and 20.

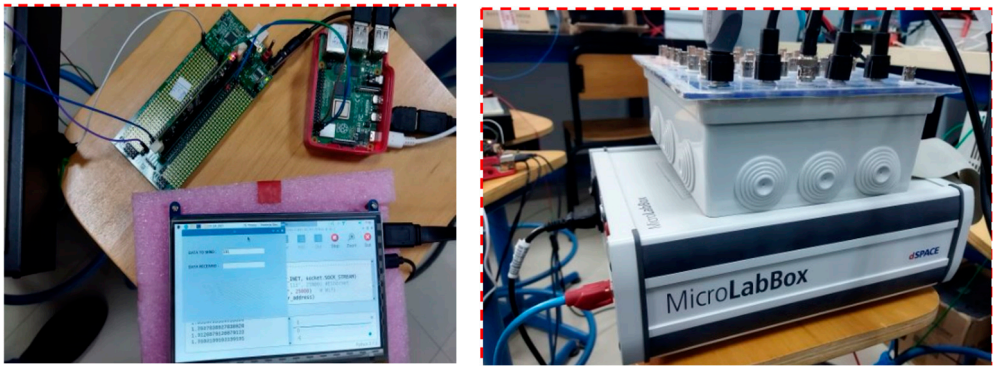


Figure 20. MicroLabBox data acquisition board and Raspberry Pi4 communication board.

The coils have been positioned arbitrarily as shown in Figure 19. This positioning leads to an efficiency of approximately 89.32%This value of the efficiency gives rise, as shown in Figure 21, to average DC reference currents of 0.6 A and 1.3 A. Note that these correspond, respectively, to the desired battery charging reference currents of 1 A and 2 A. Figure 22 shows that the battery charging current tracks well the desired reference which means that the controller ensures good tracking performances.

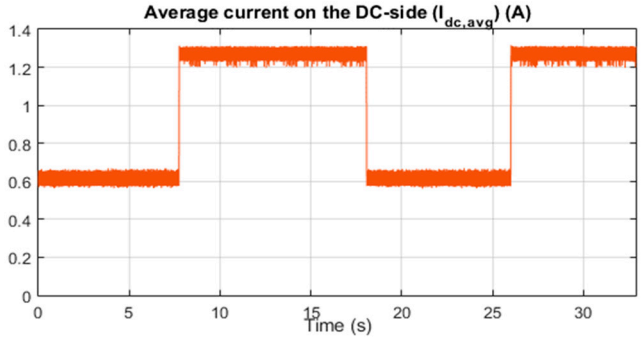


Figure 21. Average current on the DC side $I_{DC,avg}$.

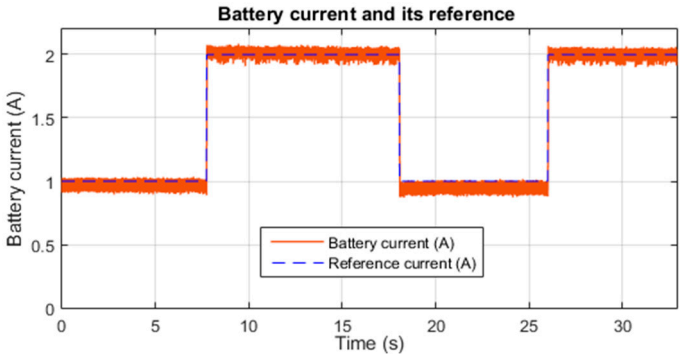


Figure 22. Battery current and its reference.

The battery voltage and DC side voltage are plotted in Figures 23 and 24. It should be noted that the used 100 V DC side voltage source is not a well-stabilized source as is shown in Figure 18. Indeed, the voltage of the latter drops from approximately 98 V to 92 V when the average DC side current passes from 0.6 A to 1.3 A. Figures 25 and 26 show the input and output power which vary according to the reference current of the WPT charger in the case of a large air gap of 250 mm in the challenging situation of loss of communication with the vehicle; also, the efficiency remains constant around a value of approximately 89.32%

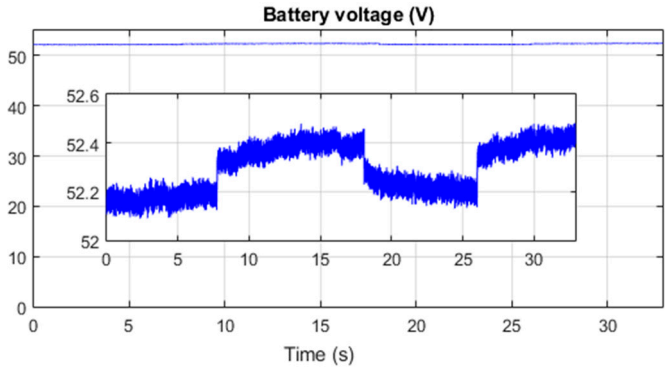


Figure 23. Battery voltage.

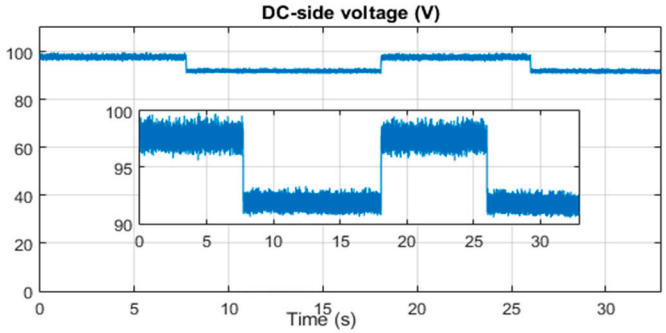


Figure 24. Correspondent DC-side voltage.

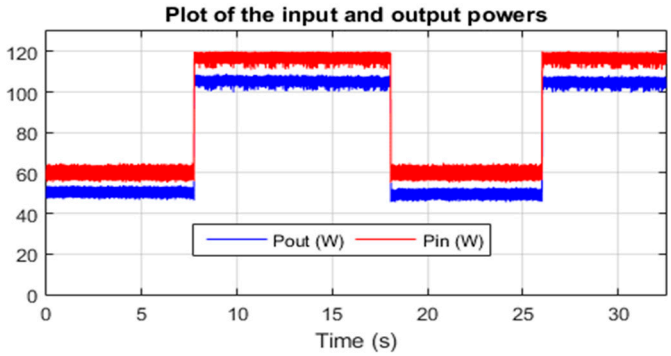


Figure 25. Output and input power.

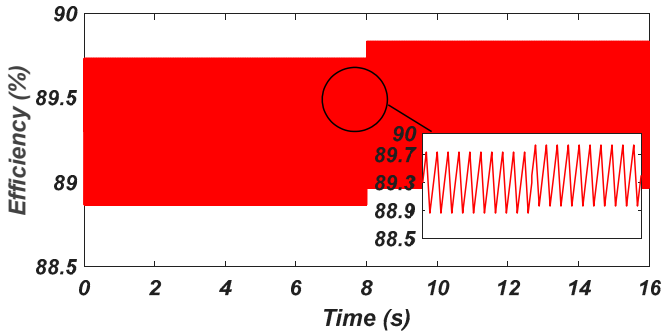


Figure 26. Corresponding efficiency.

This experimental validation is crucial because it provides empirical evidence to verify theoretical models, simulations, and hypotheses, thus guaranteeing their accuracy and reliability, and because it also brings us closer to the reality of things to see phenomena not studied or neglected in the theoretical framework or simulation. It demonstrates the

practical feasibility of proposed concepts, bridges the gap between theory and real-world applications, and identifies unforeseen problems or limitations.

6. Discussion

Our new approach allows wireless charging of the EV battery which goes in the direction of encouraging the large-scale use of EVs instead of classic combustion engine vehicles with all that goes with pollution and climate change, because, with the WPT technology, we give users convenience and safe experience with this free cable charging method, also for the future of smart cars and smart transportation without the need of the presence of drivers to charge these vehicles, and we can imagine the impact of this in the whole supply chain management, and this can be applicable from light-duty vehicle to heavy-duty vehicles such as buses or camions, and also research now are in going for underwater and space using WPT. Also, the proposed method enables system control from the ground side without additional DC-DC converters on the vehicle side, reducing system complexity and cost; the proposed method exhibits broad applicability and can be effectively employed in various WPT topologies, including (Series–Parallel) SP, Parallel–Parallel (PP), LCC-LCC and LCC-S compensation configurations.

Controlling a battery's charging current is essential to ensure its safety, longevity, and optimum performance, particularly in EVs. Excessive charging current can lead to overheating, accelerated degradation, and even thermal runaway, posing significant safety risks such as fire or explosion. By regulating the charging current within safe limits, the battery is protected against overcharging, stress, and damage, prolonging its life and maintaining its efficiency. In EVs, where batteries are critical and expensive components, this control is essential to ensure reliable operation, enhance user safety, and prevent catastrophic failure, ultimately contributing to the vehicle's durability and sustainability.

Under normal circumstances, the system operates with a wireless communication link between the ground side and the vehicle side. This means that at any given moment, the battery current is measured and transmitted wirelessly to the ground side, where the controller compares this value with the desired reference and adjusts the phase shift consequently. The phase shift, in turn, controls the inverter's MOSFETs on the ground side.

The new contribution of our approach lies in scenarios where the wireless transmission of information, in particular, battery current measurement, is interrupted due to faulty communication links, environmental interference, noise, or any other factor likely to cause a loss of wireless communication between the two sides. In such cases, our method relies on measurements taken on the primary side, which means current and voltage on the DC side, and uses an ANN to estimate system efficiency. This estimate indirectly determines the battery current, enabling the controller to adapt the phase shift control accordingly, even in the absence of direct feedback from the secondary side.

For this reason, this approach enables current to be controlled in real-life scenarios, considering the type of wireless charger, misalignment between coils generates irregularities in the voltage picked up by the secondary coil, which affects charging current and efficiency, and changes in the gap between coils disrupt the system, not to mention grid instability. The ANN estimator gives the right value of the efficiency to calculate the DC average current to keep the charging current constant, despite communication delays or even shutdowns.

Compared to existing approaches in the literature, this method fills the gap for systems that use continuous communication for data transfer and current measurement, but also for systems that use free communication between VSA and GSA, which sometimes loses this communication and can even lead to instability of the whole system. The combination of ANN and GA allows us to obtain satisfactory results that show the success of

the method under real-time conditions, as demonstrated by the simulation results and experimental validation.

7. Conclusions

This paper presented a new approach to primary-side control of a WPT charger for EVs. The method uses a GA for online gain adjustment of the PI controller combined with a feedforward ANN. The proposed approach significantly improves power transfer efficiency and system stability. Simulation results demonstrate the effectiveness of this new approach, with an efficiency of 89.32% in challenging situations of loss of communication with the vehicle. To validate the design procedure, an experimental prototype was built, operating at an operational frequency of 85 kHz. The experimental results confirm the proposed control strategy. These results underline the potential of the proposed approach for WPT applications, especially in areas with bad communication between VSA and GSA; also, the integration of AI in control systems can lead to better use of ML to improve performances in such systems. Future research directions could include the exploration of integrating renewable energy sources to build a green wireless charging infrastructure in real-world challenges. In addition, future research into fast charging techniques for WPT systems will be crucial for reducing charging times, particularly for heavy-duty vehicles. Also, exploring the possibility of hybridization of two optimization algorithms: a faster algorithm to effectively reduce search limits, and a more precise algorithm to accurately determine optimal solutions.

Author Contributions: Conceptualization, M.E.A. and A.L.; methodology, H.E.F.; software, Y.E.A.; validation, M.E.A., A.L. and H.E.F.; formal analysis, S.N.; investigation, AL. and H.E.F.; resources, H.E.F.; data curation, A.L. and A.H.; writing—original draft preparation, M.E.A. and A.L.; writing—review and editing, M.E.A., A.L. and H.E.F.; visualization, S.N. and Y.E.A.; supervision, H.E.F. and A.L.; project administration, H.E.F. All authors have read and agreed to the published version of the manuscript.

Funding: This research received no external funding.

Institutional Review Board Statement: Not applicable.

Informed Consent Statement: Not applicable.

Data Availability Statement: The original contributions presented in the study are included in the article. Further inquiries can be directed to the corresponding authors.

Conflicts of Interest: The authors declare no conflicts of interest.

References

1. Gabric, A.J. The Climate Change Crisis: A Review of Its Causes and Possible Responses. *Atmosphere* **2023**, *14*, 1081. [CrossRef]
2. Rocha, J.; Oliveira, S.; Viana, C.M.; Ribeiro, A.I. Chapter 8-Climate Change and Its Impacts on Health, Environment and Economy. In *One Health*; Prata, J.C., Ribeiro, A.I., Rocha-Santos, T., Eds.; Academic Press: Cambridge, MA, USA, 2022; pp. 253–279, ISBN 978-0-12-822794-7.
3. Binsuwadan, J. Transport Sector Emissions and Environmental Sustainability: Empirical Evidence from GCC Economies. *Sustainability* **2024**, *16*, 10760. [CrossRef]
4. Goldstein, H. The Greening of Transportation: We'll Need New Inventions and Novel Adaptations to Decarbonize the Sector. *IEEE Spectr.* **2024**, *61*, 2. [CrossRef]
5. Ferrer, A.L.C.; Thomé, A.M.T. Carbon Emissions in Transportation: A Synthesis Framework. *Sustainability* **2023**, *15*, 8475. [CrossRef]
6. Ghahramani, M.; Pilla, F. Analysis of Carbon Dioxide Emissions From Road Transport Using Taxi Trips. *IEEE Access* **2021**, *9*, 98573–98580. [CrossRef]
7. Piracha, A.; Chaudhary, M.T. Urban Air Pollution, Urban Heat Island and Human Health: A Review of the Literature. *Sustainability* **2022**, *14*, 9234. [CrossRef]

8. Bustaffa, E.; Redini, M.; Minichilli, F. Assessment of Mortality Attributable to Air Pollution in the Urban Area of Pisa (Central Italy) Characterized by Multi-Source Exposures. *Atmosphere* **2024**, *15*, 1311. [CrossRef]
9. Ali, Q.; Di Silvestre, M.L.; Lombardi, P.A.; Riva Sanseverino, E.; Zizzo, G. Electrifying the Road to Net-Zero: Implications of Electric Vehicles and Carbon Emission Coefficient Factors in European Power Systems. *Sustainability* **2024**, *16*, 5084. [CrossRef]
10. Yılmaz, H.; Yagmahan, B. Optimization of the Electric Vehicle Charging Strategy Problem for Sustainable Intercity Travels with Multiple Refueling Stops. *Sustain. Energy Grids Netw.* **2024**, *40*, 101546. [CrossRef]
11. Zentani, A.; Almaktoof, A.; Kahn, M.T. A Comprehensive Review of Developments in Electric Vehicles Fast Charging Technology. *Appl. Sci.* **2024**, *14*, 4728. [CrossRef]
12. Laha, A.; Kalathy, A.; Pahlevani, M.; Jain, P. A Comprehensive Review on Wireless Power Transfer Systems for Charging Portable Electronics. *Eng* **2023**, *4*, 1023–1057. [CrossRef]
13. Sun, X.; Xu, X.; Lin, K.; Chen, S.-E.; Zhao, T. Static and Dynamic Analysis of Wireless Power Transfer for Battery-Electric Locomotives. In Proceedings of the 2024 IEEE Transportation Electrification Conference and Expo (ITEC), Chicago, IL, USA, 19–21 June 2024; pp. 1–6.
14. Sari, V. Design and Implementation of a Wireless Power Transfer System for Electric Vehicles. *World Electr. Veh. J.* **2024**, *15*, 110. [CrossRef]
15. Rajiv, A.; Shree, R.; Rohit Bhatt, P.; Islam, B. Renewable Energy Mechanisms: An Examination of the Progress Achieved in Wireless Power Transmission Techniques. *Meas. Sens.* **2024**, *34*, 101249. [CrossRef]
16. Lassioui, A.; El Ancary, M.; El Idrissi, Z.; El Fadil, H.; Rachid, K.; Rachid, A. Primary-Side Indirect Control of the Battery Charging Current in a Wireless Power Transfer Charger Using Adaptive Hill-Climbing Control Technique. *Processes* **2024**, *12*, 1264. [CrossRef]
17. Unal, K.; Bal, G.; Oncu, S.; Ozturk, N. MPPT Design for PV-Powered WPT System with Irregular Pulse Density Modulation. *Electr. Power Compon. Syst.* **2023**, *51*, 83–91. [CrossRef]
18. Chen, J.; Hu, Z.; Wang, S.; Cheng, Y.; Liu, M. Investigation of Wireless Power Transfer for Smart Grid On-Line Monitoring Devices under HV Condition. *Procedia Comput. Sci.* **2016**, *83*, 1307–1312. [CrossRef]
19. Venkatesan, M.; Narayanamoorthi, R.; Kacor, P.; Vrzala, M. Bidirectional Wireless Power Transfer: Bridging Electric Vehicles and the Grid through Converter Analysis, Coil Topologies, and Communication Protocol Review. *Results Eng.* **2024**, *25*, 103803. [CrossRef]
20. Bertoluzzo, M.; Giacomuzzi, S.; Kumar, A. Design of a Bidirectional Wireless Power Transfer System for Vehicle-to-Home Applications. *Vehicles* **2021**, *3*, 406–425. [CrossRef]
21. *SAE J2954*; J2954 (WIP) Wireless Power Transfer for Light and Medium Duty Vehicles-SAE International. SAE International: Warrendale, PA, USA, 2024.
22. Sagar, A.; Kashyap, A.; Nasab, M.A.; Padmanaban, S.; Bertoluzzo, M.; Kumar, A.; Blaabjerg, F. A Comprehensive Review of the Recent Development of Wireless Power Transfer Technologies for Electric Vehicle Charging Systems. *IEEE Access* **2023**, *11*, 83703–83751. [CrossRef]
23. Yenil, V.; Çetin, S. Constant Voltage Control of a Secondary Side Controlled Wireless Power Transfer Converter Using LC/S Compensation. *Pamukkale Üniversitesi Mühendis. Bilim. Derg.* **2022**, *28*, 668–675. [CrossRef]
24. Zhang, Y.; Shen, Z.; Wu, Y.; Wang, H.; Pan, W. Dual-Side Phase-Shift Control for Strongly Coupled Series–Series Compensated Electric Vehicle Wireless Charging Systems. *World Electr. Veh. J.* **2022**, *13*, 6. [CrossRef]
25. Chen, W.; Liu, Z.; Liu, J.; Ye, J.; Su, H. A New Simultaneous Wireless Power and Information Transfer System With Integrated Signal Magnetic Coupler. *IEEE Trans. Ind. Electron.* **2023**, *70*, 12708–12718. [CrossRef]
26. Huang, C.-C.; Lin, C.-L.; Wu, Y.-K. Simultaneous Wireless Power/Data Transfer for Electric Vehicle Charging. *IEEE Trans. Ind. Electron.* **2017**, *64*, 682–690. [CrossRef]
27. Kalat, S.N.; Vaez-Zadeh, S.; Zakerian, A.; Babaki, A.; Ebel, T. A Communication-Free and Model-Free Predictive Control for a Dynamic IPT System With High Power Factor for Electric Vehicles. *IEEE Access* **2023**, *11*, 96773–96783. [CrossRef]
28. Kim, M.; Joo, D.-M.; Lee, B.K. Design and Control of Inductive Power Transfer System for Electric Vehicles Considering Wide Variation of Output Voltage and Coupling Coefficient. *IEEE Trans. Power Electron.* **2019**, *34*, 1197–1208. [CrossRef]
29. Yang, Y.; Zeng, J.; Hui, S.Y.R. A Fast Primary-Side Current and Voltage Control for Direct Wireless Battery Chargers. *IEEE J. Emerg. Sel. Top. Power Electron.* **2024**, *12*, 355–366. [CrossRef]
30. Chen, G.; Rao, C.; Sun, Y.; Chen, Z.; Tang, C.; Zhang, Z. Primary Control Method of Wireless Charging System Based on Load Characteristics. *Energies* **2019**, *12*, 1269. [CrossRef]
31. Xue, M.; Lu, K.; Zhu, L. Research on Load and Mutual Inductance Identification Method of WPT System Based on a LCC-S Type Compensation Network. *World Electr. Veh. J.* **2021**, *12*, 197. [CrossRef]
32. Bagheri, A.; Erfanian, A.; Abrishamifar, A. A Systematic Methodology for Optimal Design of Wireless Power Transfer System Using Genetic Algorithm. *Energies* **2020**, *13*, 383. [CrossRef]

33. Prosen, N.; Domajnko, J. Optimization of a Circular Planar Spiral Wireless Power Transfer Coil Using a Genetic Algorithm. *Electronics* **2024**, *13*, 978. [CrossRef]
34. Abdelrahim, M.; Almakhles, D. Observer-Based Control of Inductive Wireless Power Transfer System Using Genetic Algorithm. *Processes* **2023**, *11*, 1859. [CrossRef]
35. He, L.; Zhao, S.; Wang, X.; Lee, C.-K. Artificial Neural Network-Based Parameter Identification Method for Wireless Power Transfer Systems. *Electronics* **2022**, *11*, 1415. [CrossRef]
36. Zhang, H.; Liao, M.; He, L.; Lee, C.-K. Parameter Optimization of Wireless Power Transfer Based on Machine Learning. *Electronics* **2024**, *13*, 103. [CrossRef]
37. Bertoluzzo, M.; Di Barba, P.; Forzan, M.; Mognaschi, M.E.; Sieni, E. A Deep Learning Approach to Improve the Control of Dynamic Wireless Power Transfer Systems. *Energies* **2023**, *16*, 7865. [CrossRef]
38. El Ancary, M.; Lassioui, A.; El Fadil, H.; Bouanou, T.; El Idrissi, Z.; Rachid, A.; Hasni, A.; El Asri, Y. Control of a Wireless Power Transfer Charger Powered by Renewable Energies. In Proceedings of the 2024 4th International Conference on Innovative Research in Applied Science, Engineering and Technology (IRASET), Fez, Morocco, 16–17 May 2024; pp. 1–6.
39. Lassioui, A.; Elancary, M.; El Fadil, H.; El Idrissi, Z.; Bouanou, T.; Rachid, K.; Rachid, A.; Koundi, M. Output Feedback Control of a WPT Charger Based on Sliding Mode and High Gain Observer. In Proceedings of the 2024 4th International Conference on Innovative Research in Applied Science, Engineering and Technology (IRASET), Fez, Morocco, 16–17 May 2024; pp. 1–6.
40. Kiyani, M.; Abdollahi, S.E.; Baigzadehnoe, B.; Abdollahi, S.R. A Fast and Structurally Simple Control Scheme Based on a Fuzzy Supervisory Approach for Wireless Power Transfer Systems. *IET Power Electron.* **2024**, *17*, 953–961. [CrossRef]
41. Tran, H.K.; Son, H.H.; Duc, P.V.; Trang, T.T.; Nguyen, H.-N. Improved Genetic Algorithm Tuning Controller Design for Autonomous Hovercraft. *Processes* **2020**, *8*, 66. [CrossRef]
42. Mahfoud, S.; Derouich, A.; EL Ouanjli, N.; EL Mahfoud, M.; Taoussi, M. A New Strategy-Based PID Controller Optimized by Genetic Algorithm for DTC of the Doubly Fed Induction Motor. *Systems* **2021**, *9*, 37. [CrossRef]
43. Neves, T.G.; de Araújo Neto, A.P.; Sales, F.A.; Vasconcelos, L.G.S.; Brito, R.P. ANN-Based Intelligent Control System for Simultaneous Feed Disturbances Rejection and Product Specification Changes in Extractive Distillation Process. *Sep. Purif. Technol.* **2021**, *259*, 118104. [CrossRef]
44. Rajamanickam, N.; Shanmugam, Y.; Jayaraman, R.; Petrov, J.; Vavra, L.; Gono, R. Review of Compensation Topologies Power Converters Coil Structure and Architectures for Dynamic Wireless Charging System for Electric Vehicle. *Energies* **2024**, *17*, 3858. [CrossRef]
45. Yang, L.; Geng, Z.; Jiang, S.; Wang, C. Analysis and Design of an S/PS−Compensated WPT System with Constant Current and Constant Voltage Charging. *Electronics* **2022**, *11*, 1488. [CrossRef]
46. Bentalhik, I.; Lassioui, A.; EL Fadil, H.; Bouanou, T.; Rachid, A.; EL Idrissi, Z.; Hamed, A.M. Analysis, Design and Realization of a Wireless Power Transfer Charger for Electric Vehicles: Theoretical Approach and Experimental Results. *World Electr. Veh. J.* **2022**, *13*, 121. [CrossRef]

Disclaimer/Publisher's Note: The statements, opinions and data contained in all publications are solely those of the individual author(s) and contributor(s) and not of MDPI and/or the editor(s). MDPI and/or the editor(s) disclaim responsibility for any injury to people or property resulting from any ideas, methods, instructions or products referred to in the content.